

RGB-D Salient Object Detection with Ubiquitous Target Awareness

Yifan Zhao[†], Jiawei Zhao[†], Jia Li, *Senior Member, IEEE*, and Xiaowu Chen, *Senior Member, IEEE*

Abstract—Conventional RGB-D salient object detection methods aim to leverage depth as complementary information to find the salient regions in both modalities. However, the salient object detection results heavily rely on the quality of captured depth data which sometimes are unavailable. In this work, we make the first attempt to solve the RGB-D salient object detection problem with a novel depth-awareness framework. This framework only relies on RGB data in the testing phase, utilizing captured depth data as supervision for representation learning. To construct our framework as well as achieving accurate salient detection results, we propose a Ubiquitous Target Awareness (UTA) network to solve three important challenges in RGB-D SOD task: 1) a depth awareness module to excavate depth information and to mine ambiguous regions via adaptive depth-error weights, 2) a spatial-aware cross-modal interaction and a channel-aware cross-level interaction, exploiting the low-level boundary cues and amplifying high-level salient channels, and 3) a gated multi-scale predictor module to perceive the object saliency in different contextual scales. Besides its high performance, our proposed UTA network is depth-free for inference and runs in real-time with 43 FPS. Experimental evidence demonstrates that our proposed network not only surpasses the state-of-the-art methods on five public RGB-D SOD benchmarks by a large margin, but also verifies its extensibility on five public RGB SOD benchmarks.

Index Terms—RGB-D Salient Object Detection, Depth-awareness, Real-time, Ubiquitous Target Awareness.

I. INTRODUCTION

Salient object detection (SOD) aims at detecting and segmenting objects that attract human attention most visually. With the proposals of large datasets [2]–[7] and deep learning techniques [8], [9], recent works have made significant progress in accurately segmenting salient objects, which can serve as an important prerequisite for a wide range of computer vision tasks, including semantic segmentation [10], visual tracking [11], and image retrieval [12].

Recent years have witnessed significant progress in the field of salient object detection. Previous works [13]–[22] take only the RGB information as inputs, which are relatively lightweight and can be trained end-to-end. However, the reasoning of salient regions cannot be well solved when there exist multiple contrasting region proposals or ambiguous object contours. Therefore, the depth information can serve as complementary guidance to deduct the overlapping

objects, which is beneficial to salient object detection tasks. Combing the RGB information with auxiliary depth inputs, recent research efforts [1], [23]–[31], [31]–[38] have verified its effectiveness in improving the object segmentation process. These methods usually introduce an additional depth stream to encode depth maps and then fuse the RGB stream with depth stream to deduct the salient objects. For example, Piao *et al.* [39] propose a two-stream network and fuse paired multi-level features to refine the final saliency results. Zhao *et al.* [17] propose a fluid pyramid integration strategy to exploit enhanced depth features. Although promising improvements have been made, existing works mainly focus on the extraction of depth information and fusion strategies of multiple modalities. Rethinking this problem from another perspective, we, in particular, consider three challenges in RGB-D salient object detection.

The first challenge is how to make the SOD network be aware of depth information. There exist some drawbacks in conventional RGB-D SOD methods. On the one hand, these conventional methods usually rely on auxiliary branches to extract depth features and then fuse these features with RGB ones. This would lead to heavy computation burdens and insufficient modality fusion. On the other hand, object segmentation processes heavily rely on the acquisition of depth maps, which are unavailable on some extreme occasions or realistic applications. Unlike these methods, we make the first attempt to leverage depth data as additional training constraints, which do not rely on depth inputs in the testing phase, namely depth-awareness salient object detection. Taking the essence and discarding the dregs of RGB and RGB-D methods, we propose a depth-awareness module to regularize network features being aware of depth knowledge. This can be conducted in a multi-task learning trend when learning saliency detection and estimating depth maps simultaneously. Although the estimated depth awareness map is not as highly accurate as the captured one in Fig. 1, but focuses on more contrastive depth regions, which is more desirable for SOD tasks. Second, the estimated depth awareness can be taken as an indicator to mine ambiguous regions. We calculate the logarithmic error between the estimated map and groundtruth depth to generate an adaptive weight map in Fig. 1 (a). The network is further regularized to pay more attention to pixels with higher error-weighted responses, hence some semantic confusions can be gradually corrected.

The second challenge is to explore low-level cues for cross-modality interaction, *i.e.*, boundary awareness. Networks could be confused when encountering ambiguous regions in both RGB and depth data. These confusions would lead to fuzzy in-

[†]Y. Zhao and J. Zhao contribute equally to this work.

Y. Zhao, J. Zhao, J. Li and X. Chen are with the State Key Laboratory of Virtual Reality Technology and Systems, School of Computer Science and Engineering, Beihang University, Beijing, 100191, China.

J. Li and X. Chen are also with the Peng Cheng Laboratory, Shenzhen, 518000, China.

J. Li is the corresponding author (E-mail: jiali@buaa.edu.cn).

A preliminary version of this research appeared at ACM MM 2020 [1].

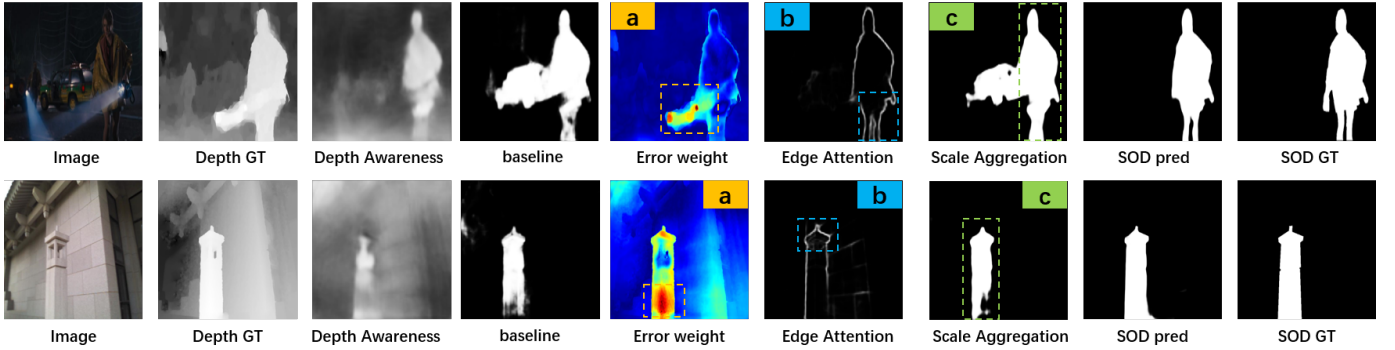


Fig. 1. Illustration of our Ubiquitous Target Awareness (UTA) network, consisting of three meaningful designs. (a) depth awareness: focusing on depth regions and mining ambiguous regions by the generated error weights between predicted depth and depth groundtruth. (b) low-level cues awareness: embedding the edge information for cross-modal fusion. (c) scale awareness: perceiving multi-scale contextual information for saliency detection.

intermediate features when fusing the features from depth modal and RGB modal. Aggregating these features progressively may finally lead to inferior saliency results. Therefore, to make clear object boundaries for saliency detection, we introduce an edge attention module¹ for cross-modality fusion in Fig. 1 b). Features should be aware of sharp boundaries to enhance their confidence in ambiguous regions. In addition, unlike previous works using simple summation or multiplication [40], [41] for cross-modality fusions, we introduce depth features as attention weights to enhance the RGB features, finding the consensus salient regions in both modalities.

The third challenge relates to the fact that salient regions are invariant in multi-scale features. Due to the intrinsic flaw of CNN in perceiving multi-scale objects, previous works [42] propose to re-scale the input image and ensemble the multi-scale output results. Besides, pyramid spatial pooling [43] offers another way by resampling the same feature layer into different scales. Despite the time-consuming issues, we found these techniques could not provide stable improvements in preferable saliency results. To tackle the scale issue in the RGB-D SOD problem, we provide an innovative Gated Multi-Scale (GMS) predictor, which employs multi-scale predictors with a gated selection in Fig. 1 c). We first re-sample the image at multiple scales and make each predictor identically map with one input scale. In the inference stage, these predictors are simultaneously activated and fused with the original branch to form a multi-scale output. Besides its notable improvements, our proposed GMS can be plug-and-play into different network architectures and introduces less additional computation cost.

In this paper, we present a real-time Ubiquitous Target Awareness (UTA) network, leveraging the advantage of depth information, multi-scale, and low-level cues. As shown in Fig. 3, we first propose to adopt a depth-awareness constraint to regularize the features in different levels of the network stage while learning the object segmentation in the meantime. This forces the segmentation features to be aware of contrastive objects in the depth of field. On the other hand, we utilize a depth error-weighted map to emphasize the saliency ambiguous regions, *i.e.*, objects salient in depth maps but not in RGB

images. These regions are attached with more attention in the overall learning procedure for alleviating the object confusion and generating clear object shapes. Based on this awareness of depth modality, we propose a novel Spatial Perceptive Module (SPM) for cross-modal fusion, which is composed of two essential parts. The first depth spatial attention provides guidance to the RGB stream, focusing and selecting common features. And the second part regularizes the fused features to be aware of sharp boundaries, generating distinct salient regions. For intra-modality fusion strategies, we propose a selective Channel-Aware Fusion (CAF) module to strengthen salient consensus features. With all these informative modules combined, we finally propose a gated multi-scale predictor to handle the multi-scale object existences.

Contributions of this paper are summarized as follows:

- 1) We first set out a novel depth-aware setting for RGB-D salient object detection and propose a Ubiquitous Target Awareness network to solve this important problem.
- 2) We propose a depth awareness module to facilitate the understanding of saliency and design a depth-aware error-weighted loss to mine ambiguous pixels.
- 3) We propose a channel-aware fusion module to adaptively select cross-level features and a spatial perceptive module to capitalize on depth-aware and low-level cues for cross-modal fusion.
- 4) We propose an effective gated multi-scale predictor to further boost performance with the mutual complementation of multi-scale features.
- 5) We conduct extensive experiments on 10 benchmarks to demonstrate the superiority of our real-time framework in promoting RGB-D SOD tasks with only RGB inputs and validate its extensibility on RGB SOD tasks with estimated training depth.

The remainder of this paper is organized as follows: Section II reviews related works and Section III describes the proposed ubiquitous target awareness network for RGB-D salient object detection. Qualitative and quantitative experiments are reported in Section IV. Section V finally concludes this paper.

II. RELATED WORK

In this section, we first review the related works about the RGB-D salient object detection and analyze the differences of our work. As our proposed method can also adapt to handling the RGB scenarios, we briefly introduce the development of

¹We use the terms boundary and edge interchangeably for better notation.

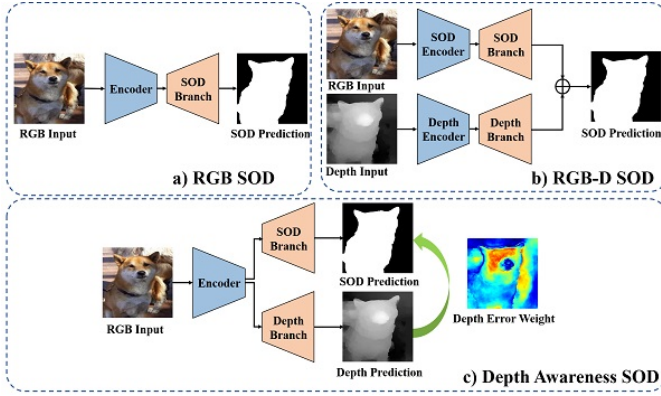


Fig. 2. Different types of SOD architecture. a): Typical RGB SOD network architecture. b): Typical RGB-D SOD network architecture. c): Proposed Depth-awareness SOD network architecture.

RGB SOD methods. At last, we review the recent works in the field of depth estimation.

RGB-D Salient Object Detection. It is shown that depth cues play an important and effective role in salient object detection. Besides methods [44], [45] utilizing hand-crafted features, recent ideas [1], [23]–[36] propose to utilize deep models to learn prior knowledge from these two different modalities. As in Fig. 2 b), existing RGB-D SOD models mainly rely on extracting salient features from RGB image and depth map respectively, and then fuse them in the early or late network stages [46]. Following this trend, earlier work [3] proposes to concatenate RGB-D pairs as 4-channel inputs for salient object detection. Considering the modality difference of depth and RGB data, Han *et al.* [47] propose a two-stream network to extract RGB features and depth features, and then fuse them with a combination layer. Piao *et al.* [39] develop a two-stream network and fuse paired multi-level side-out features to refine the final salient object detection results. To extract the informative cues from both modalities, Li *et al.* [32] propose a spatial-aware selection and a channel-aware selection module to fuse the RGB and depth features.

However, directly fusing the depth cues and RGB information would lead to insufficient cross-modality understanding. Several works [17], [24], [37], [48] propose to fuse these two modality encoders with a stage-wise or hierarchical manner. For example, Chen *et al.* [24] propose a progressive fusion strategy in a coarse-to-fine manner for sufficient information learning. Zhao *et al.* [17] propose a fluid pyramid integration strategy to make full use of depth enhanced features. Li *et al.* [48] tends to utilize the alternate interaction of different network stages for learning relations of different modalities. Besides these fusion strategies, Chen [34] propose to find a disentangled feature representation of each modality and learns to interact the same type of disentangled feature with others. Different from these aforementioned deep models, in this paper, we propose a new depth-awareness framework that does not rely on the depth data during the testing phase and learns the prior depth knowledge during training time.

RGB Salient Object Detection. Conventional RGB SOD methods tends to hand-crafted features such as color con-

straints [49], texture [5] and local/global region contrast [50]. Recently, CNN-based RGB SOD methods [13]–[22] have achieved impressive improvements over non-deep learning methods [5], [49], [50]. Most of them are designed in end-to-end architectures in Fig. 2 a). For example, Liu *et al.* [13] utilize pixel-wise contextual attention to select global and local contextual information. Zhao *et al.* [17] propose a pyramid feature attention network, which adopts channel-wise attention and spatial attention to focus more on valuable features. Wei *et al.* [20] propose a cross-feature module to fuse features of different levels and propose a boundary-sensitive loss for feature regularization. Besides, some recent works [19], [51], [52] also focus on the discovering the edge information when segmenting salient objects.

Single Image Depth Estimation. Methods of depth estimation can be divided into three groups: monocular video [53], stereo image pairs [54] and single image [55]–[59]. With the development of deep networks [8], [60], methods of depth information estimation [55]–[57] or enhancement [61] has been boosted to a new accuracy level. Eigen *et al.* [55], [56] propose a CNN-based framework for single image depth estimation, utilizing a stage-wise multi-scale network for further refinement. As an important cue in computer vision tasks, recent works tend to utilize multi-task learning to joint depth estimation and other pixel-level prediction tasks, such as semantic segmentation [62], surface normal prediction [59].

III. METHODOLOGY

A. Overview

In this section, we introduce a novel Ubiquitous Target Awareness (UTA) network for RGB-D salient object detection. The main idea of our framework is to leverage depth, multi-scale, and low-level spatial constraints to regularize the feature learning process. These regularizations are naturally embedded in one unified network, endowing the learned features to be aware of specific representations.

Motivation of Depth-awareness SOD. As mentioned above, conventional RGB-D methods adopt an RGB encoder for the three-channel RGB input while using a depth encoder to encode the captured depth image. Then the extracted features are fused together to get the final output. However, this learning manner leaves a major concern: is depth information always useful for salient object detection?

In Fig. 4, the quality of captured depth maps varies greatly under different circumstances. These phenomena are inevitable considering the various imaging conditions. From the low quality to high quality of depth images, it would lead to different learning manners of salient object detection tasks. The high-quality depth maps usually provide explicit low-level cues, involving boundaries, textures, and color contrasts. However, the low-quality depth maps in the first row of Fig. 4 provide noisy information for salient object learning. Existing works utilize the depth data in a consistent manner and regard it as positive information under all circumstances. However, when facing the depth data of low-quality, these methods would incorporate noisy inputs and harm the SOD learning performance.

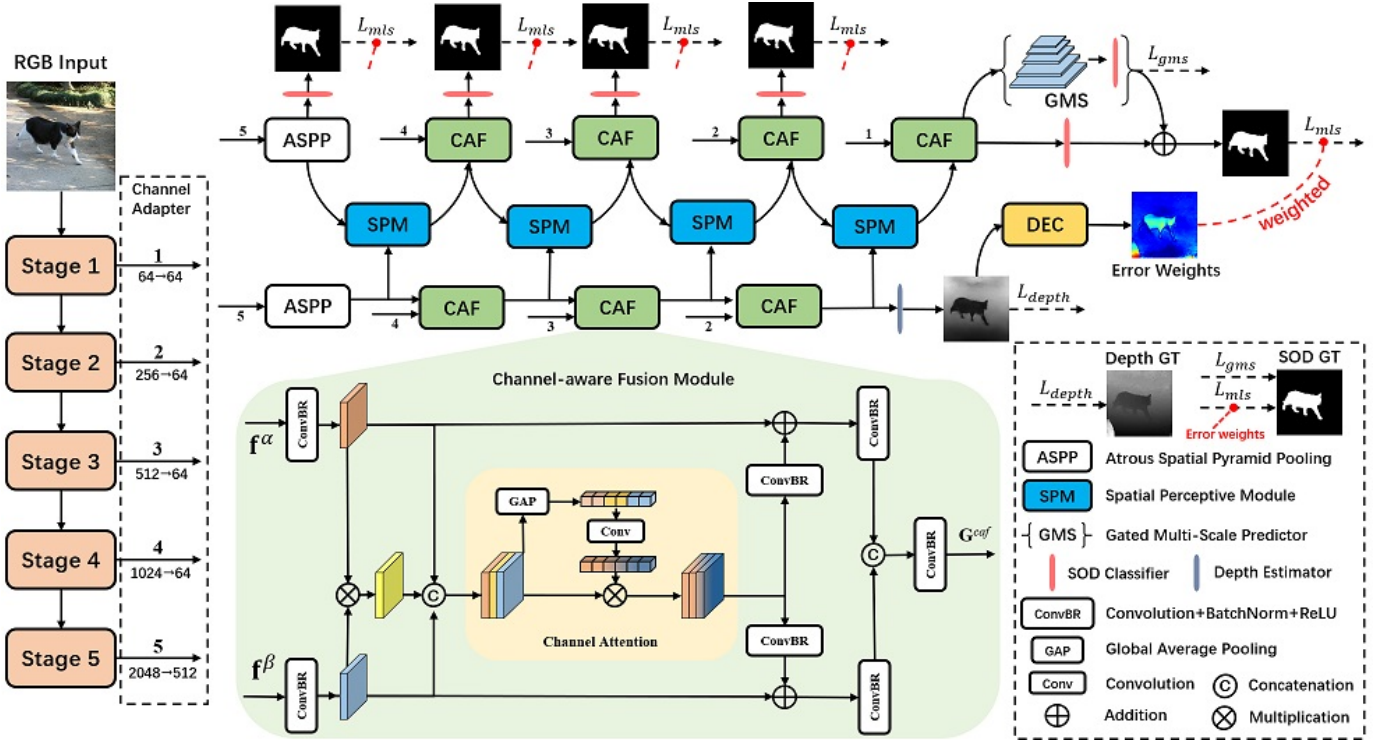


Fig. 3. The overall architecture of our proposed Ubiquitous Target Awareness (UTA) network, which introduces three awareness into network embedding. 1) depth awareness: introducing depth supervision and depth error-weighted correction (DEC) module. 2) low-level cues awareness: spatial perceptive module (SPM) for cross-modality fusion with boundary supervision. 3) scale awareness: introducing a plug-and-play gated multi-scale (GMS) module. In each modality, a channel-aware fusion module (CAF) is proposed to select the channel-wise salient consensus features.

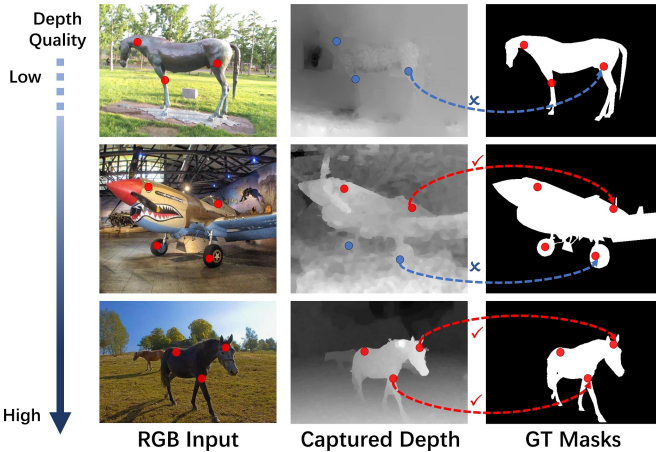


Fig. 4. The motivation of depth-awareness SOD. Depth maps of high quality can provide clear low-level cues for SOD learning while the low-quality ones usually introduce noisy information. The red and blue dotted lines indicate the positive and negative effects on the learning process respectively.

To solve this important problem, we explore the depth data as a learnable prior knowledge rather than directly encoding the raw depth data. This designment shows following advantages: 1) The estimated depth data plays a stable and positive role in complementing the RGB branch and their quality would not be restricted by the imaging condition. 2) We propose to correct the errors in the depth-saliency ambiguous regions,

where should be attach more importance during the learning process. 3) Our framework takes only RGB data as input, while not relies on the capture of depth data. This advantage greatly extends our framework into some extreme scenarios without clear depth data, or in single-modal RGB applications.

Architecture of Depth-awareness SOD. Let I_{RGB} , I_D and M denote the input RGB image, depth data and SOD mask respectively. \mathcal{E} and \mathcal{D} denotes the encoder and decoder network in SOD architecture. Conventional RGB SOD methods in Fig. 2 a) takes only RGB images as input, *i.e.*, $M = \mathcal{D}(\mathcal{E}(I_{RGB}))$. With depth maps as auxiliary inputs in Fig. 2 b), the overall framework requires two independent encoders to extract the depth and RGB features separately, which main computation costs are usually lied in. Methods of this category [38], [63] can be similarly denoted as $M = \mathcal{D}_R(\mathcal{E}_R(I_{RGB})) \uplus \mathcal{D}_D(\mathcal{E}_D(I_D))$, where \uplus denotes the cross modal fusion strategies. Moreover, the depth and RGB encoders are separately trained and the relationships between these multi-modal data are not fully explored. Taking only RGB inputs as well as saving the computation costs, the depth-aware salient object detection in Fig. 2 c) provides us a new perspective to utilize the depth data in this segmentation task. In the testing phase, the network only takes the RGB as input and the object segmentation results are regularized by the depth-awareness constraints in the training phase. This testing process can be represented as $M = \mathcal{D}_R(\mathcal{E}(I_{RGB})) \uplus \mathcal{D}_D(\mathcal{E}(I_{RGB}))$, where \mathcal{D}_D is supervised by captured depth groundtruth.

In this framework, after the weight-sharing encoder network, we propose a depth-awareness branch to predict the depth information in Fig. 3. Thus depth features in this auxiliary branch benefiting SOD in two aspects: 1) passing into the depth-error correction (DEC) to help mine ambiguous regions; 2) serving as depth modality data to enhance and fuse with the original RGB branch. For the cross-modality fusion, we propose a spatial perceptive module (SPM) to force SOD features to be aware of depth data and boundary cues. For the fusion of intra-modality, we present a channel-aware fusion module, finding salient consensus features and alleviating the noisy ones. After that, we propose a plug-and-play gated multi-scale predictor (GMS) to perceive the multi-scale object existences. Benefiting from the ubiquitous target awareness, our framework does not rely on depth data or edge information in the testing phase, generating high-quality segmentation masks with intrinsic features.

B. Depth-awareness Constraint

What role does depth information play in salient object detection? To answer this question, in this paper, we propose an innovative depth-awareness constraint from two complementary aspects, *i.e.*, multi-level depth awareness, and depth error-weighted correction. These two aspects work collaboratively to regularize the salient features being aware of contrastive depth regions and contextual salient confusions, which facilitate the segmentation process in different learning stages.

Multi-level Depth Awareness. As discussed in previous works [24], [38], [64], the key issue in salient object detection lies in the utilization of multi-level features in different network stages. Besides the aggregation strategy, the other exploitation is to regularize the features focusing on meaningful regions, which provides useful contextual information before aggregation. Taking the advantages of depth information and the hierarchical network architecture, we force the segmentation features to focus on depth regions in different network learning stages, which is elaborated in Fig. 3. This means in each network learning stage, features should be aware of the object information as well as depth-contrastive regions. We use an additional depth branch to regress the groundtruth depth. With this collaborative learning of SOD and depth regression, we further fuse these two branches to refine the salient object detection results (see Fig. 3), which builds strong correlations between these two different types of features. Notably, this refinement strategy can also be well handled by the spatial perceptive module (SPM), with additional boundary supervision at multiple levels. As a result, the salient features stand as a predominant place in the final optimization and the depth maps become leading guidance.

Depth Error-weighted Correction. To make thorough exploitation of depth information, we further propose a depth error-weighted correction (DEC) to regularize hard pixels with higher weights where the predicted depth makes mistakes. As it stands, the network itself naturally tends to be highly responded to the salient regions and then form a holistic salient object. However, this would guide the predicted depth features focusing on salient regions, resulting in a severe

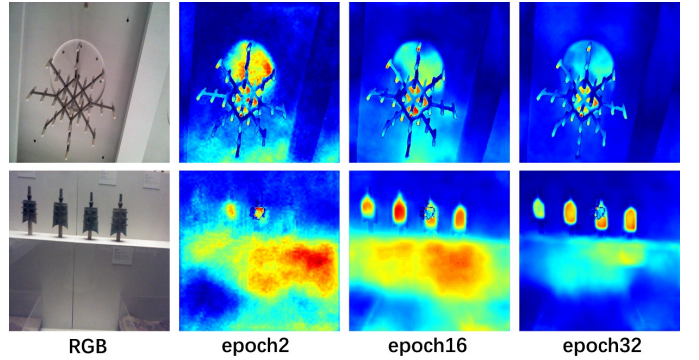


Fig. 5. Qualitative visualization of depth error weights in different training epochs. The ambiguous error regions can be iteratively optimized during the training process.

misalignment between the predicted depth and groundtruth data. Remarkably, the error regions where the predicted depth makes mistakes are usually the semantic ambiguous regions, which we need to pay more attention to in the learning process.

In order to solve this misalignment as well as to exploit it, we thus introduce a logarithmic depth error weight. Let p^d and y^d be the predicted depth and depth groundtruth (GT) respectively, the error weight e_{ij} of each pixel has the form:

$$e_{ij} = \frac{\sum_{i=1}^h \sum_{j=1}^w (\log p_{ij}^d - \log y_{ij}^d)}{\sum_{i=1}^h \sum_{j=1}^w \max(\log p^d - \log y^d)}, \quad (1)$$

where w and h are the width and height of the error window, which represents the error of central pixel with the mean value of local regions. In this way, the ambiguous pixels are treated with more attention in the early learning phase. As the optimization goes through, the regularized features become depth-aware, and errors are progressively corrected. This learning progress is exhibited in Fig. 5, where the highly-responded regions in the error map shrink along with the learning stage. This verifies that the final optimized features are aware of depth information and better at handling semantic confusions.

C. Channel-aware Cross-level Interaction

The crucial problem in salient object detection is to select the most discriminative features and to pass them in a coarse-to-fine scheme. However, aggregating features from different levels in an encoder-decoder fashion usually leads to missing details or introduces ambiguous features, which jointly lead to a bad network optimization. Besides, high-level features show a strong ability to capture salient regions but fail to generate finer boundaries, while low-level features contain boundary and detailed cues but also more noisy features.

Toward this end, we propose a novel Channel-Aware Fusion module (CAF), which adaptively selects the discriminative features for object understanding. The proposed CAF shows some meaningful designs, which are illustrated in Fig. 3. First, given two types of source feature $\mathbf{f}^\alpha, \mathbf{f}^\beta \in \mathbb{R}^{W' \times H' \times C'}$, we use pixel-wise multiplication to enhance the common pixels in feature maps, while alleviating the ambiguous ones. The

enhanced features are then concatenated with the transformed features with a lightweight encoder $\mathcal{E}(\cdot)$. This operation can be formally represented as:

$$\mathbf{f}^{ca} = \mathcal{E}_\alpha(\mathbf{f}^\alpha) \odot \mathcal{E}_\beta(\mathbf{f}^\beta) \odot (\mathcal{E}_\alpha(\mathbf{f}^\alpha) \otimes \mathcal{E}_\beta(\mathbf{f}^\beta)), \quad (2)$$

where \odot and \otimes denote the feature concatenation operation and pixel-wise multiplication respectively. Each encoder $\mathcal{E}_{\{\alpha,\beta\}}$ is typically composed of a 3×3 convolutional layer followed by a Batch Normalization and a ReLU activation. Especially, when aggregating the multi-level features, the features \mathbf{f}^α and \mathbf{f}^β are first upsampled to the same scale, which is omitted for better view in Fig. 3.

After obtaining rich feature $\mathbf{f}^{ca} \in \mathbb{R}^{W' \times H' \times 3C'}$ by Eq. (2), the second main concern is how to select the most relevant features that are highly-responded in the segmentation target. Inspired by the channel-attention mechanism [65], [66], we thus propose to use global features for a contextual understanding of the attention weights. The \mathbf{f}^c is squeezed with a global average pooling, followed by a sigmoid normalization σ , and is then transformed as the vector shape to align the channel dimension with the original feature. This serialized operation has the form:

$$\mathbf{a} = \frac{1}{W' \times H'} \sum_{i=1}^{W'} \sum_{j=1}^{H'} \mathbf{f}_{i,j}^{ca}, \quad (3)$$

$$\mathbf{u}_{i,j,k} = \mathbf{f}_{i,j,k}^{ca} \otimes \sigma(\varphi(\mathbf{a}_k)). \quad (4)$$

φ is a linear transformation to reorganize the pooling features and \mathbf{u} denotes the learned attention weighted features. Therefore features relevant to the salient target could be prominent in each group of source features \mathbf{f}^α and \mathbf{f}^β . This can be achieved by a channel-aware attention mechanism:

$$\mathbf{G}^{caf} = \mathcal{R}_g(\mathcal{E}_{v1}(\mathcal{E}_\alpha(\mathbf{f}^\alpha) \oplus \mathcal{R}_{u1}(\mathbf{u})) \odot \mathcal{E}_{v2}(\mathcal{E}_\beta(\mathbf{f}^\beta) \oplus \mathcal{R}_{u2}(\mathbf{u}))), \quad (5)$$

where $\mathcal{R}_{\{u1,u2,g\}}$ denotes the typical shape-preserving decoder and $\mathcal{E}_{\{v1,v2\}}$ denotes the dimensional reduction decoder, forming a same shape as original inputs. Hence the relevant features to target object can be enhanced in the final output \mathbf{G}^{caf} . In addition, to implement the whole framework in a lightweight trend, the channel dimension C' is empirically set as 64 to achieve state-of-the-art performance.

D. Spatial-aware Cross-modal Interaction

In this subsection, we propose a spatial perceptive module (SPM) to handle the cross-modal interaction of depth data and RGB data. Unlike the above-mentioned fusion strategies, we propose to enhance the feature representation using two attention modules, *i.e.*, depth spatial attention and edge spatial attention. The cross-modal fusion first aims to find the saliency consensus in both depth and RGB data. As complementation to RGB data, we leverage the normalized depth attention map as guidance to help the saliency inference. With given RGB features \mathbf{f}^{RGB} and depth features \mathbf{f}^D , this operation could be formally represented as:

$$\mathbf{f}^{dsa} = (\mathbf{f}^{RGB} \otimes \sigma(\mathbf{f}^D) \oplus \mathbf{f}^{RGB}) \odot \mathbf{f}^D, \quad (6)$$

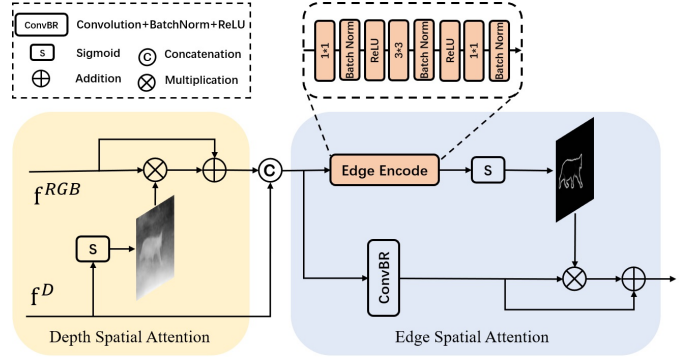


Fig. 6. Illustration of the proposed Spatial Perceptive Module (SPM) for cross-modal interaction. Features from the RGB stream are first enhanced with depth attention to find the salient coherent regions and then fed into an edge spatial attention module to incorporate the low-level cues in the fusion process.

where \mathbf{f}^{dsa} denotes the depth-enhanced feature with spatial-aware depth attentions, and $\sigma(\cdot)$ is the sigmoid normalization. On the other hand, although depth data provide high-level saliency guidance for the fused features, low-level cues are usually neglected during the message passing. In addition, depth data are sometimes captured in low-quality, progressively fusion with multi-stage decoders would aggravate this phenomenon. Thus we introduce the boundary information as the low-level guidance to form a clear object shape. To explicitly embed the edge features into the network, we use a feature encoder \mathcal{E}_{edge} consisting of 1×1 , 3×3 and 1×1 convolutional blocks with BatchNorm and ReLU supervised by edge masks. The salient boundaries are generated by canny edge detectors and expanded to a width of five pixels.

With the encoded edge features, we then pass them with a sigmoid function to generate normalized attention maps. The depth-enhanced features \mathbf{f}^{dsa} pass by a convolutional block \mathcal{R}_s to reduce its channels and conduct a pixel-wise spatial attention mechanism:

$$\mathbf{G}_{i,j}^{spm} = (\mathcal{R}_s(\mathbf{f}_{i,j}^{dsa}) \otimes \sigma(\mathcal{E}_{edge}(\mathbf{f}_{i,j}^{dsa}))) \oplus \mathcal{R}_s(\mathbf{f}_{i,j}^{dsa}). \quad (7)$$

The proposed SPM modules are embedded in multiple cross-modal fusion stages. Progressively employing this module helps keep the low-level details in the network learning stage, which is beneficial to generate sharp masks.

E. Gated Multi-Scale Predictor

There is a natural defect in deep CNNs to perceive multi-scale features, due to the fixed down-sample and up-sample operations. In particular we consider two predominant approaches in tackling this issue: 1) multi-scale inference (MSI) [42]: ensembling outputs of multi-scale inputs, *e.g.*, rescaled from 0.5 to 2.0 during inference; 2) pyramid pooling module (PPM) [17], [43]: pooling the feature map to multiple scales of the same layer. These two operations are precisely exhibited in Fig. 7.

Here we elaborate on these methods in tackling SOD tasks: multi-scale inference techniques suppose that objects should be relatively salient despite their scales. However, once the

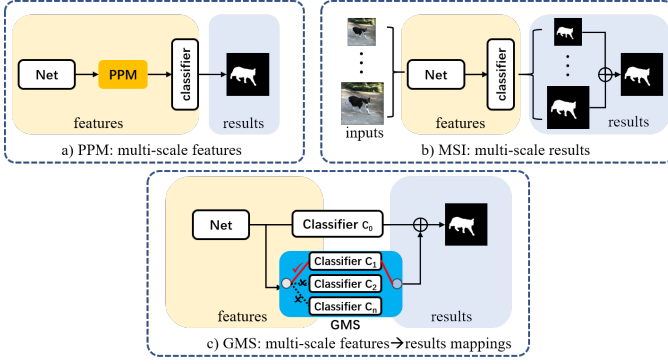


Fig. 7. Comparisons of three multi-scale strategies. a) PPM [43]: aggregating multi-scale features to the new feature. b) MSI [42]: aggregating multi-scale results to the new result. c) proposed GMS: naturally embedded in network prediction and transforming features to results.

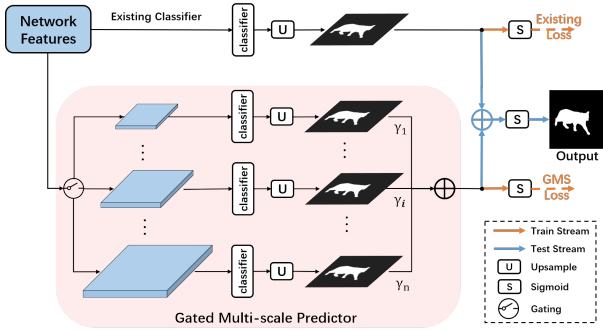


Fig. 8. Illustration of the proposed Gated Multi-Scale (GMS) predictor. Multiple individual classifiers with 1×1 linear transformations are adopted to grasp the scale-related features. The existing loss in our manuscript denotes the previously defined loss in Eqn. (16), *i.e.*, \mathcal{L}_{depth} , \mathcal{L}_{edge} , \mathcal{L}_{mfs} .

network is optimized, the understanding of salient objects is usually fixed. This relative saliency relationship is hard to obtain. Besides MSI, the pyramid pooling module (PPM) [43] introduces variant scales by resizing the feature map of the same layer. By introducing additional computation costs, the reception field of the same pixel could be enlarged.

Different from these above methods, we propose a new gated multi-scale predictor in Fig. 8, which provides several technical insights in salient object detection. We observe that it is the last SOD classification layer that affects the result mostly. Before that, rich features of multiple scales are contained in a high dimension of $\mathbb{R}^{W \times H \times C}$. The final classification layer aims to excavate the most reliable SOD map $\mathbb{R}^{W \times H \times 1}$ from these features, which can be regarded as a mapping function \mathcal{F} . However, this operation is conducted into a single-scale trend. When object scales change, this learned single classifier conducts the same mapping function \mathcal{F} , leading to inferior results.

Essentially speaking, the final mapping function \mathcal{F} would significantly affect the quality of salient object detection. The mapping function is composed of two operations, *i.e.*, a rescaling operation and a 3×3 convolutional layer. Thus we propose to use multi-scale predictors with a set of mapping functions, *i.e.*, $\mathcal{F}^1, \mathcal{F}^2, \dots, \mathcal{F}^n$ of n scales. In the training

phase, we rescale the input image to different sizes, *i.e.*, [224, 256, 288, 320, 352]. When images of one scale are fed into the network, only one scale predictor and the backbone classifier are activated, which are controlled by a gating function. In the testing phase, only one scale of input is fed into the network, and all mapping functions are activated to perceive a multi-scale saliency understanding. The output features are finally weighted for summation in Fig. 8 and then fused with the existing classifier. The weights γ is set as [0.25, 0.25, 0.25, 0.25, 1] for five GMS branches respectively. Moreover, our proposed GMS is a plug-and-play module in parallel with the existing SOD classifier, which is lightweight and can further boost the performance based on preferable results.

F. Learning Objective

As a typical SOD task, our framework is first supervised with the SOD masks, with a typical Binary Cross-Entropy (BCE) loss. Let $p^s, y^s \in \mathbb{R}^{W \times H \times 1}$ be the predicted salient mask and corresponding groundtruth, the BCE loss has the form:

$$\mathcal{L}_{bce} = - \sum_{i=1}^H \sum_{j=1}^W y_{ij}^s \log(p_{ij}^s). \quad (8)$$

However, the BCE loss usually leads to noisy predictions which do not form a holistic object. To make the salient object with clear boundaries, we adopt an Intersection over Union (IoU) measurement [19], [20] as the auxiliary loss:

$$\mathcal{L}_{iou} = 1 - \frac{\sum_{i=1}^H \sum_{j=1}^W (y_{ij}^s \times p_{ij}^s) + 1}{\sum_{i=1}^H \sum_{j=1}^W (y_{ij}^s + p_{ij}^s - y_{ij}^s \times p_{ij}^s) + 1}. \quad (9)$$

Beyond the SOD supervision, our learning objective is supervised by multiple constraints, as in Fig. 3, the depth awareness module, the error-weighted correction, the auxiliary edge supervision for cross-modality fusion, and the scale-awareness constraints. For the first depth-awareness constraint, we adopt the logarithmic Mean Square Error (logMSE) for supervision [55], [56] to generate smooth depth maps, and meanwhile providing the error weights:

$$\mathcal{L}_{depth} = \frac{1}{W \times H} \sum_{i=1}^H \sum_{j=1}^W \|\log y_{ij}^d - \log p_{ij}^d\|_2^2. \quad (10)$$

For edge encoders in the spatial perceptive module, we adopt a BCE loss to predict edges as a binary classification task:

$$\mathcal{L}_{bce}^{edge} = - \sum_{i=1}^H \sum_{j=1}^W y_{ij}^e \log(p_{ij}^e), \quad (11)$$

where y_{ij}^e and p_{ij}^e denote the edge labels and predicted edges respectively. Then with four SPM modules, the final summation loss \mathcal{L}_{edge} can be represented as:

$$\mathcal{L}_{edge} = \sum_{e=1}^4 \mathcal{L}_{bce}^{edge}. \quad (12)$$

For the error-weighted correction, we adopt an error-weighted BCE loss to attach more importance to the wrongly-predicted pixels:

$$\mathcal{L}_{dec} = \frac{-\sum_{i=1}^H \sum_{j=1}^W \mathbf{e}_{ij} \times y_{ij}^s \log(p_{ij}^s)}{\sum_{i=1}^H \sum_{j=1}^W \mathbf{e}_{ij}}. \quad (13)$$

This error loss \mathcal{L}_{dec} adopts the same SOD groundtruth masks y_{ij}^s . To implement the multi-level supervision in a unified framework, the multi-level loss \mathcal{L}_{mls} can be formulated as:

$$\mathcal{L}_{mls} = \sum_{i=1}^S \lambda_i (\mathcal{L}_{bce} + \mathcal{L}_{iou} + \mathcal{L}_{dec}), \quad (14)$$

where λ_i denotes the weights of multi-level losses and S is set as 5 representing five stages in ResNet. Here we follow GCPANet [67] and set λ as [1, 0.8, 0.6, 0.4, 0.2].

For the gated multi-scale predictor of the final S stages, we adopt an auxiliary loss \mathcal{L}_{gms} to learn scale-aware information:

$$\mathcal{L}_{gms} = \mathcal{L}_{bce} + \mathcal{L}_{iou} + \mathcal{L}_{dec}. \quad (15)$$

With the above regularizations combined, the overall loss function \mathcal{L}_{sum} can be formulated as:

$$\mathcal{L}_{sum} = \mathcal{L}_{depth} + \mathcal{L}_{edge} + \mathcal{L}_{mls} + \mathcal{L}_{gms}. \quad (16)$$

IV. EXPERIMENTS

A. Datasets and Evaluation Metrics

RGB-D SOD Datasets. To evaluate the performance of the proposed approach, we conduct experiments on five RGB-D benchmarks [2]–[4], [40], [68], including NJUD [2] with 1,985 images captured by Fuji W3 stereo camera, NLPR [3] with 1,000 images captured by Kinect, STEREO [4] with 1,000 images collected from the Internet, DES [40] with 135 images captured by Kinect, SIP [28] with 929 images of human activities captured by Huawei Mate10. Following previous works [37], [39], we split 1,500 samples from NJUD and 700 samples from the NLPR dataset for training, the rest images in these two datasets and the other three datasets for testing.

RGB SOD Datasets. To verify the effectiveness of our method on RGB datasets, we adopt five RGB benchmarks [5]–[7], [69], [70], including DUTS [7] with 15,572 images, ECSSD [5] with 1,000 images, DUT-OMRON [69] with 5,168 images, PASCAL-S [70] with 850 images, HKU-IS [6] with 4,447 images. DUTS is currently the largest SOD dataset, following [7], we split 10,553 images (DUT-TR) from DUTS for training and 5,019 images (DUT-TE) from DUTS for testing, the other four datasets are also used for testing.

Evaluation Metrics. To quantitatively evaluate the performance of our approach and state-of-the-art methods, we adopt 4 commonly used metrics: max F-measure (F_{β}^{max}), mean F-measure (F_{β}^{mean}), weighted F-measure (F_{β}^w), mean absolute error (MAE), Precision-Recall (PR) curve and F-measure curve on both RGB methods and RGB-D methods.

Following previous works [1], We use F_{β} to measure both Precision and Recall. F_{β} is computed based on Precision and Recall pairs as follows:

$$F_{\beta} = \frac{(1 + \beta^2) \times Precision \times Recall}{\beta^2 \times Precision + Recall}, \quad (17)$$

where we set $\beta^2=0.3$ to emphasize more on Precision than Recall, and compute F_{β}^{max} , F_{β}^{mean} and F_{β}^w using different thresholds as in [71].

B. Implementation Details

We adopt ResNet-50 [8] pre-trained on ImageNet [72] dataset as our backbone. The atrous rate of ASPP follows the prior work [73], which is set as (2, 4, 6). In the training stage, we resize each image to 352×352 and rescale them with the width of [224, 256, 288, 320, 352] for GMS training. Besides, we adopt horizontal flipping, random cropping for data augmentation. We use the SGD optimizer with the batch size=32 for 48 epochs. Inspired by [20], [67], we adopt warm-up and linear decay strategies to adjust the learning rate with the maximum learning rate of 0.005 for ResNet-50 backbone and 0.05 for others. We set the momentum and decay rate as 0.9 and $5e-4$ respectively. Our model is lightweight and all experiments are conducted on a single NVIDIA 1080Ti GPU. The error window size is set as 1 for simplicity.

For the RGB-D SOD, we utilize both RGB images and depth maps from training sets to train our model. During the testing stage, we only need RGB images as inputs to predict saliency maps on RGB-D test sets. For the RGB SOD task, we first estimate depth maps for DUT-TR by pre-trained VNLNet [59] directly, which works well in the single image depth estimation task. Then we utilize both DUT-TR and its corresponding predicted depth maps to train our model. During the inference stage, we only need RGB images as inputs to predict saliency maps on RGB test sets.

C. Comparisons with the state-of-the-art

As shown in Tab. I, we compare our Ubiquitous Target Awareness (UTA) model on 5 widely-used RGB-D SOD benchmarks with 12 state-of-the-art methods, including DF [23], CTMF [47], MMCI [25], PCF [24], TANet [26], CPFP [37], DMRA [39], D3Net [28], SSF [27], CoNet [35], DCMF [34], ICNet [33]. Different from conventional RGB-D SOD methods, it is clear that our method achieves a new performance leader-board without depth images as input, which puts our model in inferior places for comparison. Especially for the F_{β}^{max} , F_{β}^{mean} and F_{β}^w metrics, our model outperforms over 3%, which means our method has a strong capability to utilize depth information for more precise saliency maps. In addition, based on our previous work (DASNet) [1], the proposed UTANet achieves higher performance on 4 benchmark datasets, while reaches comparable performance on the DES dataset. Beneficial from the design of depth-awareness architecture and lightweight implementation of the SPM, our model performs 43 images per second with a 352×352 input, reaching a satisfactory trade-off of the speed and accuracy.

In Fig. 10, we exhibit results predicted by our model and other approaches. Among these methods, our model performs best on completeness and clarity. The first row exhibit typical scenarios where the salient object is relatively hard to disentangle. Thus with the help of depth awareness, object saliency can be easily deducted. The second and third rows exploit two complex scenarios where the salient objects are confused

TABLE I

PERFORMANCE COMPARISON WITH 12 STATE-OF-THE-ART RGB-D SOD METHODS ON FIVE BENCHMARKS. SMALLER MAE , LARGER F_{β}^{max} , F_{β}^{mean} AND F_{β}^w INDICATES BETTER PERFORMANCE. RESULTS RANKED IN THE FIRST AND SECOND PLACES ARE HIGHLIGHTED IN BOLD AND UNDERLINED.

METHODS	FPS	NJUD-TE				NLPR-TE				STEREO				DES				SIP			
		F_{β}^{max}	F_{β}^{mean}	F_{β}^w	MAE	F_{β}^{max}	F_{β}^{mean}	F_{β}^w	MAE	F_{β}^{max}	F_{β}^{mean}	F_{β}^w	MAE	F_{β}^{max}	F_{β}^{mean}	F_{β}^w	MAE	F_{β}^{max}	F_{β}^{mean}	F_{β}^w	MAE
DF [23]	0.1	.804	.744	.545	.141	.778	.682	.516	.085	.757	.616	.549	.141	.766	.566	.392	.093	.704	.673	.406	.185
CTMF [47]	1.6	.845	.788	.720	.085	.825	.723	.679	.056	.831	.786	.698	.086	.844	.765	.687	.055	.720	.684	.535	.139
MMCI [25]	19	.852	.813	.739	.079	.815	.729	.676	.059	.863	.812	.760	.068	.822	.750	.650	.065	.840	.795	.712	.086
PCF [24]	15	.872	.844	.803	.059	.841	.794	.762	.044	.860	.845	.778	.064	.804	.763	.711	.049	.861	.825	.768	.071
TANet [26]	14	.874	.844	.805	.060	.863	.796	.780	.041	.861	.828	.787	.060	.827	.795	.740	.046	.851	.809	.748	.075
CPFP [37]	7	.876	.850	.828	.053	.869	.840	.807	.036	.874	.842	.817	.051	.838	.815	.787	.038	.870	.819	.788	.064
DMRA [39]	10	.886	.872	.847	.051	.879	.855	.840	.031	.868	.847	.847	.066	.888	.857	.843	.030	.847	.815	.734	.088
D3Net [28]	20	.889	.860	.833	.051	.885	.853	.826	.030	.881	.844	.815	.054	.885	.859	.831	.030	.847	.818	.793	.058
SSF [27]	32	<u>.911</u>	.886	.871	.043	.912	.873	.867	.026	.902	.880	.862	.044	.912	.882	.852	.026	-	-	-	-
CoNet [35]	<u>34</u>	.902	.872	.849	.047	.898	.848	.842	.031	.912	.885	<u>.871</u>	.040	.916	.862	.848	.027	.883	.842	.803	.063
DCMF [34]	-	.898	.859	.831	.047	.895	.839	.828	.031	.887	.841	.811	.047	.879	.812	.780	.027	.866	.819	.780	.068
ICNet [33]	13	.891	.869	.843	.052	.908	.884	.864	.028	.898	.870	.844	.035	.913	.893	.867	.027	.857	.834	.791	.069
Ours (DASNet) [1]	33	<u>.911</u>	<u>.894</u>	<u>.872</u>	<u>.042</u>	<u>.929</u>	<u>.907</u>	<u>.892</u>	<u>.021</u>	<u>.915</u>	<u>.894</u>	<u>.870</u>	<u>.037</u>	.928	.892	.867	.023	.900	.867	.836	.051
Ours (UTA)	43	.915	.903	.883	.037	.932	.917	.905	.020	.921	.905	.887	.033	<u>.922</u>	.888	.865	.024	.897	.872	.843	.048

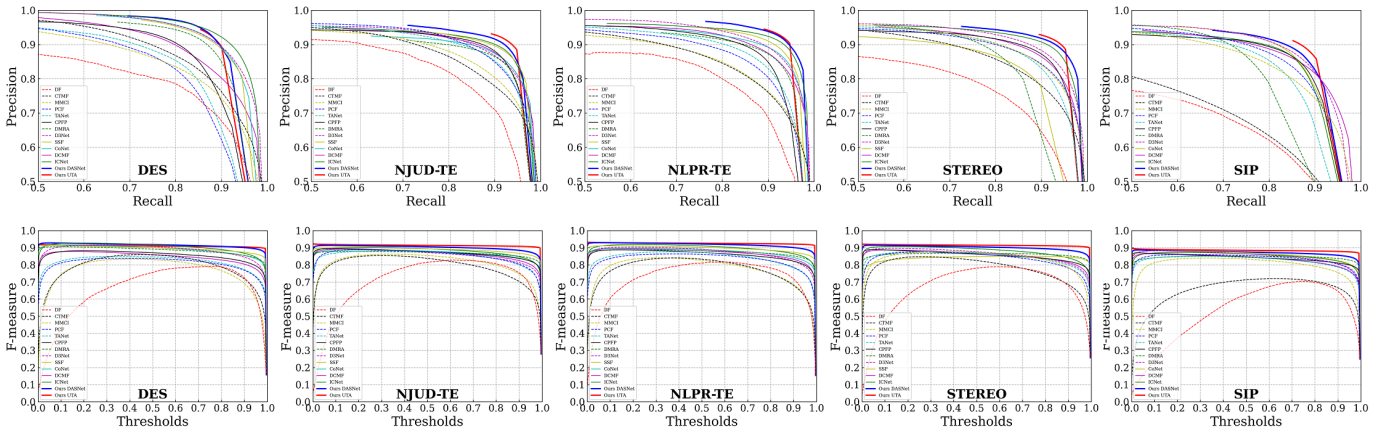


Fig. 9. The Precision-Recall curves and F-measure curves of 12 state-of-the-art models and our approaches are listed across five public benchmarks.

with the backgrounds. It can be seen that our model has the potential to detect the most salient object while alleviating ambiguous backgrounds. For the last three rows, we explore to see what will happen when models facing inferior depth input. It can be seen that simply using depth information cannot detect the holistic object boundary, thus existing models fail to judge the saliency due to their strong dependency on clear depth inputs. In other words, these models tend to give high confidence in the depth boundaries. Unlike these conventional methods, the proposed UTANet shows a clear contextual understanding of these two modalities and is simultaneously aware of low-level cues, e.g., clear depth boundaries.

D. Analysis of depth quality in RGB-D SOD

With the aforementioned phenomenon, we summarize that the unstable depth quality would provide an inferior understanding of salient objects. To verify the challenge in Fig. 4, we make an experimental study to explore the relationship between depth quality and the SOD learning process.

Evaluation setting. The clear depth groundtruth of these low-quality images cannot be directly obtained. Inspired by

existing work [28] which reduces the low-quality depth maps for learning, we define a “depth-saliency consistency” as the consistency of the transformed depth maps with the salient object detections results. In other words, if the depth map can directly predict the SOD mask, it provides useful cues for the SOD learning process. We then adopt the depth-SOD encoding network in Fig. 11 with backbone encoder and a single-branch decoder from UTANet (denoted as *Ours-Base*). In addition, the predictions of salient objects are probability distributions. Thus instead of comparing the training prediction with 0-1 groundtruth masks, we measure them with the prediction of the dual input network in Fig. 11.

To measure the “depth-saliency consistency” scores, we use the MAE metric for evaluations. In this manner, we re-partition the dataset with similarity ranking scores and extract the top 30% to 100% of the training data. We compare two different types of network: the proposed UTANet (namely depth-aware) with only RGB input for inference, and the dual input network by adding an auxiliary depth encoder on UTANet. We conduct comparisons in Tab. II on four widely-used RGB-D benchmarks. From these results, several interesting findings

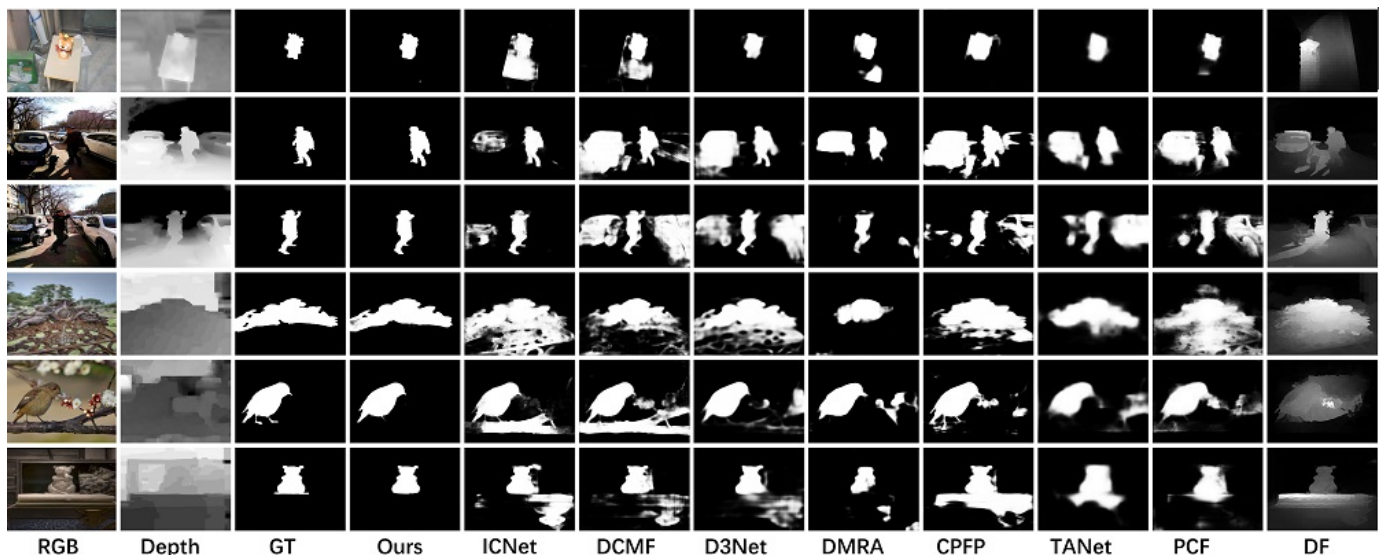


Fig. 10. Qualitative comparison of the state-of-the-art RGB-D methods and our approach. Saliency maps produced by our model are clearer and more accurate than others in various challenging scenarios.

TABLE II

PERFORMANCE COMPARISONS OF RGB-D SOD RESULTS WITH DIFFERENT PROPORTIONS OF DEPTH DATA ON 4 BENCHMARKS. TRAINING DATA ARE RANKED BY THE QUALITY OF DEPTH MAPS.

Training data	METHODS	NJUD-TE				NLPR-TE				STEREO				SIP			
		F_{β}^{max}	F_{β}^{mean}	MAE	F_{β}^w	F_{β}^{max}	F_{β}^{mean}	MAE	F_{β}^w	F_{β}^{max}	F_{β}^{mean}	MAE	F_{β}^w	F_{β}^{max}	F_{β}^{mean}	MAE	F_{β}^w
Top 30%	Ours (Depth-Aware)	.856	.830	.064	.802	.919	.902	.023	.890	.879	.854	.048	.831	.833	.796	.078	.754
	Ours (Depth GT)	.869	.844	.058	.819	.932	.920	.018	.909	.891	.864	.047	.841	.877	.846	.062	.809
Top 50%	Ours (Depth-Aware)	.879	.858	.053	.837	.826	.911	.021	.898	.890	.867	.044	.846	.855	.825	.067	.786
	Ours (Depth GT)	.911	.892	.041	.875	.935	.919	.019	.909	.905	.883	.040	.863	.892	.863	.053	.833
Top 70%	Ours (Depth-Aware)	.898	.878	.046	.857	.934	.919	.019	.907	.912	.894	.036	.876	.900	.874	.050	.842
	Ours (Depth GT)	.911	.892	.041	.875	.935	.919	.019	.909	.921	.900	.035	.882	.905	.881	.045	.854
Top 100%	Ours (Depth-Aware)	.915	.903	.037	.883	.932	.917	.020	.905	.921	.905	.033	.887	.897	.872	.048	.843
	Ours (Depth GT)	.927	.913	.034	.898	.933	.918	.019	.907	.920	.899	.034	.883	.903	.878	.048	.849

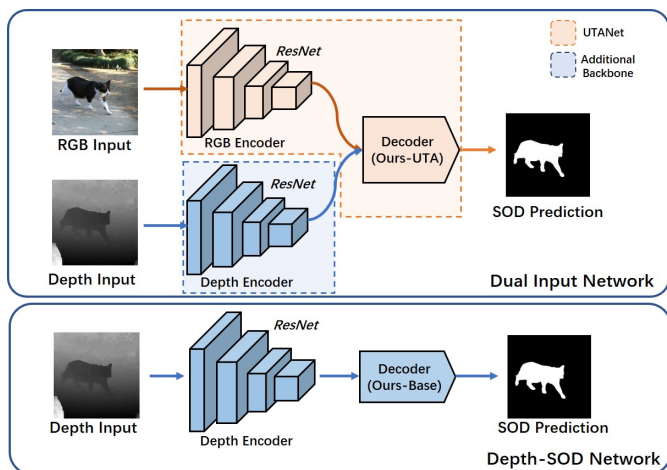


Fig. 11. Network architectures for calculating depth-saliency consistency. Dual input network indicates adding an individual encoder on UTANet to encode depth GT. The Depth-SOD network indicates using only depth information for SOD prediction.

are concluded: 1) High-quality depth data can facilitate the learning process of salient object detection. In the setting of

top 30% and 50% data, it can be found that by adding depth GT inputs with an additional encoder, the performance is improved consistently on almost all evaluation metrics. 2) With the increase of inferior depth data, the network with depth GT performs similar results with the proposed UTANet. By observing the F-max value of SIP dataset, with the accurate depth cues for SOD, the depth-awareness network performs much lower results than that with depth GT, e.g., 0.833 and 0.877 in F_{β}^{max} . However, when utilizing all training data, the performance of both settings is increased but the gap between these methods becomes close, e.g., 0.897 and 0.903 in F_{β}^{max} .

In summary, it is concluded that the proposed UTANet handles the different quality of training depth well and is independent of depth quality. While the dual input network performs well with high-quality depth data but leads to inferior results with low-quality depth data.

E. Performance Analysis

To investigate the effectiveness of each key component in our proposed model, we first conduct a thorough ablation study and then measure the computation complexity. After that, a comparison on RGB SOD benchmarks is exhibited to verify the extensibility of our model.

TABLE III

ABLATION STUDY FOR DIFFERENT COMPONENTS. CAF DENOTES THE PROPOSED CHANNEL AWARE FUSION MODULE. SPM DENOTES THE SPATIAL PERCEPTIVE MODULE, DAC DENOTES THE DEPTH AWARENESS CONSTRAINT. GMS DENOTES THE PROPOSED GATED MULTI-SCALE PREDICTOR. BCE, IoU, DEC ARE DIFFERENT LOSS FUNCTIONS MENTIONED ABOVE. MLS REPRESENTS MULTI-LEVEL SUPERVISION.

DAC	SPM	CAF	GMS	MLS	NJUD-TE			NLPR-TE			STERE			SIP			FPS
					F_{β}^{mean}	F_{β}^w	MAE	F_{β}^{mean}	F_{β}^w	MAE	F_{β}^{mean}	F_{β}^w	MAE	F_{β}^{mean}	F_{β}^w	MAE	
					.855	.830	.052	.856	.850	.029	.856	.833	.047	.826	.788	.062	80
✓					.863	.837	.051	.868	.860	.027	.867	.843	.044	.836	.799	.059	65
✓	✓				.882	.862	.042	.884	.878	.024	.887	.868	.037	.857	.823	.052	59
		✓			.880	.861	.044	.884	.876	.025	.884	.865	.038	.856	.826	.051	58
✓		✓			.889	.870	.042	.892	.880	.024	.888	.867	.038	.864	.835	.049	48
✓	✓	✓			.891	.871	.040	.908	.894	.021	.893	.874	.036	.868	.834	.049	44
✓	✓	✓	✓		.896	.875	.039	.917	.904	.020	.899	.878	.035	.874	.844	.048	43
✓	✓	✓	✓	✓	.903	.883	.037	.917	.905	.020	.905	.887	.033	.872	.843	.048	43

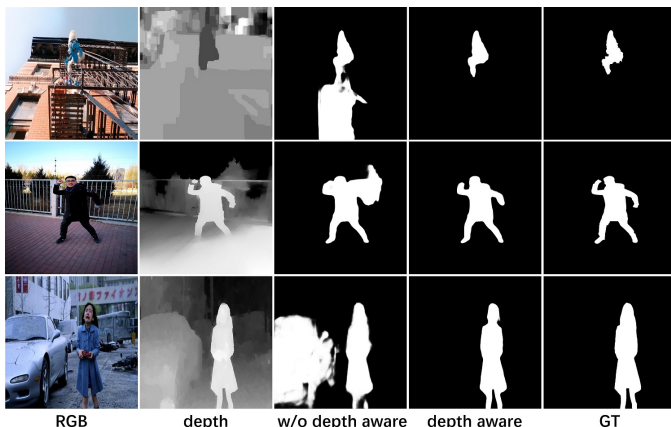


Fig. 12. Qualitative comparisons on RGB-D datasets. The third column without depth awareness is hard to distinguish complex scenarios with similar foreground and background, while our model in the fourth column shows better performance.

TABLE IV

ABLATION STUDY FOR CROSS-MODAL FUSION STRATEGIES. ALL-CAF: REPLACING SPM MODULE WITH CAF MODULE FOR CROSS-MODALITIES.

	NJUD-TE		NLPR-TE		STERE	
	F_{β}^{mean}	MAE	F_{β}^{mean}	MAE	F_{β}^{mean}	MAE
UTA (full model)	.903	.037	.917	.020	.905	.033
w/o SPM	.890	.041	.909	.020	.893	.033
All-CAF	.894	.041	.908	.022	.899	.036
w/o Edge	.897	.038	.912	.021	.898	.034

Ablation Studies. To evaluate the effectiveness of our feature fusion module, we reconstruct our model with different ablation factors in Tab. III. We first replace the cross-level fusion module with multiplication operations as our baseline in the first row, which only includes the IoU Loss and BCE loss. Note that this baseline model outperforms several state-of-the-art models and our proposed model can steadily improve the performance based on this high baseline. As an important constraint to the SOD feature, using depth awareness constraints (denoted as DAC) in a multi-task learning trend can boost the performance. Although the DAC module includes

the auxiliary depth branch and depth error correction (DEC), the relation between multiple modalities is unexplored. To solve this, we add the cross-modal fusion strategies SPM, the performance improves notably, *e.g.*, over 2% in F_{β}^{mean} and F_{β}^w measurements.

Channel-aware Cross-level Interaction. Our channel-aware cross-level interaction is denoted as CAF in Tab. III, adopting channel-aware attention is proved to be necessary for fusing and selecting channels from multiple levels, which can boost over 3% performance in F_{β}^{mean} and F_{β}^w compared to the high baseline model. At last, we add multi-level supervision to refine our results. As shown in Tab. III, all components contribute to the performance improvement, which demonstrates the necessity of each component of our proposed model to obtain the best saliency detection results.

Depth-awareness Constraints. Qualitative results can be found in Fig. 12. The SOD results with and without depth awareness constraints are presented in the third and fourth columns. It is interesting to find that simply using the RGB image, the salient objects are hard to localize, *e.g.*, the person in the first image. However, these objects are salient in the depth map and provide clear localization cues. Therefore, using depth-awareness constraints is beneficial for the salient localization in the fourth column.

Spatial-aware Cross-modal Interaction. Are spatial cues necessary for cross-modality interactions? To verify the effectiveness of our proposed spatial perceptive module, we conduct detailed ablations in Tab. IV. The first setting in the second row is to replace all SPM modules with the feature concatenation operations (denoted as w/o SPM). It can be found that the performance drop by about 1% when missing the positional information. The second setting denoted as (ALL-CAF) utilizes the efficient CAF module to replace the original SPM module, which leads to inferior performance. Last but not least, we remove the edge attention module (w/o Edge), the module achieves better performance than the first two settings but lower performance than our full model. This verifies that spatial information is thus necessary for cross-modality fusion.

Gated Multi-scale Predictor. To compare with other typical multi-scale strategies, *i.e.*, pyramid pooling module (PPM), multi-scale inference (MSI) as mentioned in Section III-E, we conduct a thorough experiment in Tab. V. It is verified

TABLE V

ABLATIONS OF THE PROPOSED GATED MULTI-SCALE PREDICTOR. THE RED ARROWS (\uparrow) AND BLUE ARROWS (\downarrow) DENOTE THE RELATIVE IMPROVEMENTS RESPECTIVELY.

Methods	NJUD-TE		NLPR-TE		STERE	
	F_{β}^{mean}	MAE	F_{β}^{mean}	MAE	F_{β}^{mean}	MAE
baseline	.855	.052	.856	.029	.856	.047
+GMS	.874(\uparrow 1.9)	.046	.886(\uparrow 3.0)	.025	.876(\uparrow 2.0)	.040
+PPM	.862(\uparrow 0.7)	.051	.868(\uparrow 1.2)	.027	.868(\uparrow 1.2)	.043
+MSI	.857(\uparrow 0.2)	.054	.848(\downarrow 0.8)	.030	.857(\uparrow 0.1)	.047
Ours w/o GMS	.898	.040	.909	.020	.897	.036
+GMS	.903(\uparrow 0.5)	.037	.917(\uparrow 0.8)	.020	.905(\uparrow 0.8)	.033
+PPM	.895(\downarrow 0.3)	.040	.900(\downarrow 0.9)	.023	.898(\uparrow 0.1)	.035
+MSI	.889(\downarrow 0.9)	.042	.899(\downarrow 1.0)	.021	.893(\downarrow 0.4)	.037
UCNet [31]	.885	.044	.884	.028	.874	.041
+GMS	.887(\uparrow 0.2)	.045	.888(\uparrow 0.4)	.027	.885(\uparrow 1.1)	.038
+PPM	.877(\downarrow 0.8)	.047	.886(\uparrow 0.2)	.027	.869(\downarrow 0.5)	.044
+MSI	.871(\downarrow 1.4)	.046	.861(\downarrow 2.3)	.031	.865(\downarrow 0.9)	.044

that both our GMS and PPM module can notably improve the quality of saliency detection results, *i.e.*, 1% of PPM and over 2% of our GMS module. In the second block, we exhibit the results of our full model without the GMS module. Based on this high-performance module, PPM and MSI fail to refine the segmentation results. As a comparison, our proposed GMS can still boost the F_{β}^{mean} by about 0.8% on this high base.

Our gated multi-scale predictor is easy to plug into the existing salient object detection networks. To verify the generalization ability of GMS, we plug our gated multi-scale predictor, pyramid pooling module, and multi-scale inference strategy into other networks respectively. The training and testing protocol follows the official code in [31]. As shown Tab. V shows, our gated multi-scale predictor could achieve an explicit improvement in all experiments and achieve higher performance than the other two multi-scale aggregation strategies. This extended experiment demonstrates the generalization ability of our gated multi-scale predictor.

Extensions on RGB SOD Benchmark. As a depth-awareness model, our testing phase does rely on the captured depth groundtruth. Thus we utilize a coarse estimated depth map for depth supervision and verify the flexibility and extensibility on RGB SOD tasks. As shown in Tab. VI, we compare our proposed UTA with 10 state-of-the-art methods, *i.e.*, BPM [74], PAGR [64], R3Net [75], PiCANet [13], PoolNet [76], BANet [18], CPDNet [15], BASNet [19], F3Net [20], and GCPANet [67]. As shown in Tab. VI, we can see our proposed UTA still outperforms other methods and ranks first on all datasets and almost all metrics. However, this performance is achieved with only estimated depth maps as training priors. we believe that with the captured real data, the final performance would be improved steadily, which is validated on the RGB-D benchmarks. As shown in Fig. 13, comparing with the visual results of different methods, our approach shows a clear superiority in both completeness and clarity. It can be found that our model precisely captures

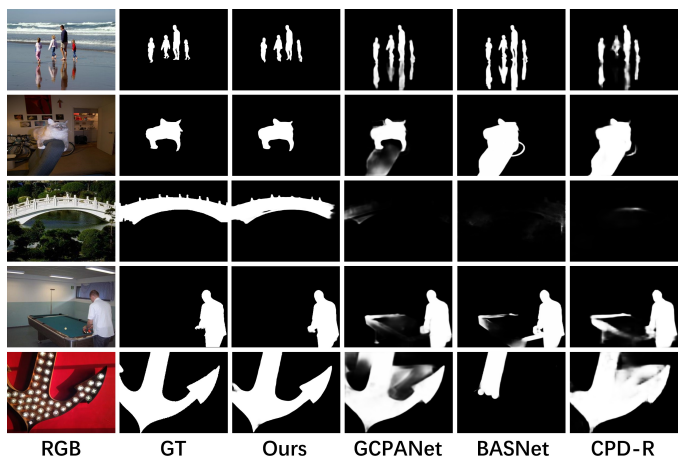


Fig. 13. Qualitative comparison of the state-of-the-art RGB methods and our approach. Obviously, saliency maps produced by our model are clearer and more accurate than others in various challenging scenarios.

the salient object and omits the background confusions.

Computational Efficiency. Tab. VII shows the parameters and computational cost measured by multiply-adds (MAdds) of our proposed model and other open-sourced RGB models and RGB-D models. Our model could achieve obvious higher performance in a lightweight fashion. Notably, SSF [27] and CPD-R [15] discard features of two shallower layers to improve the computation efficiency, but sacrifice the accuracy and clarity of results. For fair comparisons, we obtain the deployment codes released by authors and evaluate them with the same configuration.

V. CONCLUSIONS

In this paper, we revisit the problem of depth in the field of salient object detection and propose a novel depth-awareness architecture to solve this important problem. The proposed depth-awareness setting takes depth as supervision in the network learning stage, to regularize the features to be aware of depth information. Base on this architecture, we propose Ubiquitous Target Awareness (UTA) network to solve the three main challenges in RGB-D SOD tasks, *i.e.*, depth regularization and error correction, low-level cues awareness in cross-modal fusion, and multi-scale perception. The depth-awareness module first provides depth localization cues to find the saliency consensus of depth and SOD branch and generates the depth-error weights to mine salient ambiguous regions. Second, the predicted depth stream is regularized by a spatial perceptive module, being aware of boundary cues simultaneously. Besides, we propose a generalized multi-scale gating module for salient object detection, which is implementation-friendly and can be plugged into multiple existing SOD frameworks. These three modules work collaboratively to promote the learning process of salient object detection. Experimental evidence reveals that with only RGB inputs, the proposed network not only surpasses the state-of-the-art RGB-D methods by a large margin but well demonstrates its effectiveness in RGB application scenarios.

TABLE VI

PERFORMANCE COMPARISON WITH 10 STATE-OF-THE-ART RGB SOD METHODS ON FIVE BENCHMARKS. SMALLER MAE , LARGER F_{β}^{max} , F_{β}^{mean} AND F_{β}^w CORRESPOND TO BETTER PERFORMANCE. THE BEST RESULTS ARE HIGHLIGHTED IN BOLD.

METHODS	FPS	ECSSD				DUT-TE				DUT-OMRON				HKU-IS				PASCAL-S			
		F_{β}^{max}	F_{β}^{mean}	F_{β}^w	MAE	F_{β}^{max}	F_{β}^{mean}	F_{β}^w	MAE	F_{β}^{max}	F_{β}^{mean}	F_{β}^w	MAE	F_{β}^{max}	F_{β}^{mean}	F_{β}^w	MAE	F_{β}^{max}	F_{β}^{mean}	F_{β}^w	MAE
BMPM [74]	28	.929	.894	.871	.045	.851	.762	.761	.049	.774	.698	.681	.064	.921	.875	.860	.039	.862	.803	.785	.073
PAGR [64]	-	.927	.894	.834	.061	.854	.784	.724	.056	.771	.711	.622	.071	.918	.886	.823	.048	.854	.803	.738	.094
R3Net [75]	22	.934	.914	.902	.040	-	-	-	-	.795	.747	.728	.062	.915	.893	.877	.036	.842	.800	.760	.095
PiCA-R [13]	5	.935	.901	.867	.046	.860	.759	.755	.051	.803	.717	.695	.065	.919	.880	.842	.043	.867	.800	.782	.077
BANet [18]	-	.939	.917	.908	.041	.872	.829	.811	.040	.782	.750	.736	.061	.923	.893	.887	.037	.847	.839	.817	.079
PoolNet [76]	32	.944	.915	.896	.039	.880	.809	.807	.040	.808	.747	.729	.055	.933	.899	.883	.032	.869	.822	.800	.074
BASNet [19]	25	.943	.880	.904	.037	.859	.791	.803	.048	.805	.756	.751	.056	.928	.895	.890	.032	.857	.775	.800	.078
CPD-R [15]	66	.939	.917	.898	.037	.865	.805	.795	.043	.797	.747	.719	.056	.925	.891	.876	.034	.864	.824	.803	.072
F3Net [20]	-	.945	.925	.912	.033	.890	.840	.835	.035	.813	.766	.746	.053	.937	.910	.900	.028	.880	.840	.821	.064
GCPANet [67]	-	.948	.919	.903	.035	.888	.817	.821	.040	.812	.748	.734	.056	.938	.898	.889	.031	.876	.836	.816	.064
Ours (UTA)	<u>43</u>	.952	.937	.924	.030	.890	.862	.849	.035	.816	.781	.766	.048	.939	.921	.910	.026	.882	.852	.828	.064

TABLE VII

COMPLEXITY COMPARISON WITH RGB MODELS AND RGB-D MODELS. MODELS RANKING THE FIRST AND SECOND PLACE ARE VIEWED IN BOLD AND UNDERLINED.

	Methods	Platform	Params(M)	MAdds(G)	FPS
RGB&RGB-D	Ours UTA	pytorch	31.83	<u>10.27</u>	<u>43</u>
	Ours DASNet [1]	pytorch	36.68	11.57	33
RGB-D	CPFP [37]	caffe	72.94	21.25	7
	DMRA [39]	pytorch	59.66	113.09	10
	CoNet [35]	pytorch	43.86	34.39	34
	SSF [27]	pytorch	<u>32.93</u>	46.53	32
RGB	GCPANet [67]	pytorch	67.06	26.61	-
	BASNet [19]	pytorch	87.06	97.51	25
	CPD-R [15]	pytorch	47.85	7.19	66
	BANet [18]	caffe	55.90	35.83	-

ACKNOWLEDGMENT

This work was supported by grants from National Natural Science Foundation of China (No.61922006) and Baidu academic collaboration program.

REFERENCES

- J. Zhao, Y. Zhao, J. Li, and X. Chen, "Is depth really necessary for salient object detection?" in *ACM Conference on Multimedia (ACM MM)*, 2020.
- R. Ju, L. Ge, W. Geng, T. Ren, and G. Wu, "Depth saliency based on anisotropic center-surround difference," in *2014 IEEE international conference on image processing (ICIP)*. IEEE, 2014, pp. 1115–1119.
- H. Peng, B. Li, W. Xiong, W. Hu, and R. Ji, "Rgbd salient object detection: a benchmark and algorithms," in *European conference on computer vision*. Springer, 2014, pp. 92–109.
- Y. Niu, Y. Geng, X. Li, and F. Liu, "Leveraging stereopsis for saliency analysis," in *2012 IEEE Conference on Computer Vision and Pattern Recognition*. IEEE, 2012, pp. 454–461.
- Q. Yan, L. Xu, J. Shi, and J. Jia, "Hierarchical saliency detection," in *Proceedings of the IEEE conference on computer vision and pattern recognition*, 2013, pp. 1155–1162.
- G. Li and Y. Yu, "Visual saliency based on multiscale deep features," in *Proceedings of the IEEE conference on computer vision and pattern recognition*, 2015, pp. 5455–5463.
- L. Wang, H. Lu, Y. Wang, M. Feng, D. Wang, B. Yin, and X. Ruan, "Learning to detect salient objects with image-level supervision," in *Proceedings of the IEEE Conference on Computer Vision and Pattern Recognition*, 2017, pp. 136–145.
- K. He, X. Zhang, S. Ren, and J. Sun, "Deep residual learning for image recognition," in *Proceedings of the IEEE conference on computer vision and pattern recognition*, 2016, pp. 770–778.
- J. Long, E. Shelhamer, and T. Darrell, "Fully convolutional networks for semantic segmentation," in *Proceedings of the IEEE conference on computer vision and pattern recognition*, 2015, pp. 3431–3440.
- B. Lai and X. Gong, "Saliency guided dictionary learning for weakly-supervised image parsing," in *Proceedings of the IEEE Conference on Computer Vision and Pattern Recognition*, 2016, pp. 3630–3639.
- S. Hong, T. You, S. Kwak, and B. Han, "Online tracking by learning discriminative saliency map with convolutional neural network," in *International conference on machine learning*, 2015, pp. 597–606.
- L. Shao and M. Brady, "Specific object retrieval based on salient regions," *Pattern Recognition*, vol. 39, no. 10, pp. 1932–1948, 2006.
- N. Liu, J. Han, and M.-H. Yang, "Picanet: Learning pixel-wise contextual attention for saliency detection," in *Proceedings of the IEEE Conference on Computer Vision and Pattern Recognition*, 2018, pp. 3089–3098.
- G. Li, Z. Liu, R. Shi, and W. Wei, "Constrained fixation point based segmentation via deep neural network," *Neurocomputing*, vol. 368, pp. 180–187, 2019.
- Z. Wu, L. Su, and Q. Huang, "Cascaded partial decoder for fast and accurate salient object detection," in *Proceedings of the IEEE Conference on Computer Vision and Pattern Recognition*, 2019, pp. 3907–3916.
- J. Li, J. Su, C. Xia, M. Ma, and Y. Tian, "Salient object detection with purificatory mechanism and structural similarity loss," *IEEE Transactions on Image Processing*, 2021.
- T. Zhao and X. Wu, "Pyramid feature attention network for saliency detection," in *Proceedings of the IEEE Conference on Computer Vision and Pattern Recognition*, 2019, pp. 3085–3094.
- J. Su, J. Li, Y. Zhang, C. Xia, and Y. Tian, "Selectivity or invariance: Boundary-aware salient object detection," in *Proceedings of the IEEE International Conference on Computer Vision*, 2019, pp. 3799–3808.
- X. Qin, Z. Zhang, C. Huang, C. Gao, M. Dehghan, and M. Jagersand, "Basnet: Boundary-aware salient object detection," in *Proceedings of the IEEE Conference on Computer Vision and Pattern Recognition*, 2019, pp. 7479–7489.
- Q. H. Jun Wei, Shuhui Wang, "F3net: Fusion, feedback and focus for salient object detection," in *AAAI Conference on Artificial Intelligence (AAAI)*, 2020.
- C. Li, R. Cong, C. Guo, H. Li, C. Zhang, F. Zheng, and Y. Zhao, "A parallel down-up fusion network for salient object detection in optical remote sensing images," *Neurocomputing*, vol. 415, pp. 411–420, 2020.
- M. Ma, C. Xia, and J. Li, "Pyramidal feature shrinking for salient object detection," in *Proceedings of the AAAI Conference on Artificial Intelligence*, vol. 35, no. 3, 2021, pp. 2311–2318.
- L. Qu, S. He, J. Zhang, J. Tian, Y. Tang, and Q. Yang, "Rgbd salient object detection via deep fusion," *IEEE Transactions on Image Processing*, vol. 26, no. 5, pp. 2274–2285, 2017.
- H. Chen and Y. Li, "Progressively complementarity-aware fusion network for rgb-d salient object detection," in *Proceedings of the IEEE*

- conference on computer vision and pattern recognition, 2018, pp. 3051–3060.
- [25] H. Chen, Y. Li, and D. Su, “Multi-modal fusion network with multi-scale multi-path and cross-modal interactions for rgb-d salient object detection,” *Pattern Recognition*, vol. 86, pp. 376–385, 2019.
- [26] H. Chen and Y. Li, “Three-stream attention-aware network for rgb-d salient object detection,” *IEEE Transactions on Image Processing*, vol. 28, no. 6, pp. 2825–2835, 2019.
- [27] M. Zhang, W. Ren, Y. Piao, Z. Rong, and H. Lu, “Select, supplement and focus for rgb-d saliency detection,” in *IEEE Conference on Computer Vision and Pattern Recognition (CVPR)*, 2020, pp. 3472–3481.
- [28] D.-P. Fan, Z. Lin, Z. Zhang, M. Zhu, and M.-M. Cheng, “Rethinking RGB-D salient object detection: Models, datasets, and large-scale benchmarks,” *IEEE TNNLS*, 2020.
- [29] Z. Chen, R. Cong, Q. Xu, and Q. Huang, “Dpanet: Depth potentiality-aware gated attention network for rgb-d salient object detection,” *IEEE Transactions on Image Processing*, 2020.
- [30] C. Li, R. Cong, S. Kwong, J. Hou, H. Fu, G. Zhu, D. Zhang, and Q. Huang, “Asif-net: Attention steered interweave fusion network for rgb-d salient object detection,” *IEEE transactions on cybernetics*, vol. 51, no. 1, pp. 88–100, 2020.
- [31] J. Zhang, D.-P. Fan, Y. Dai, S. Anwar, F. S. Saleh, T. Zhang, and N. Barnes, “Uc-net: uncertainty inspired rgb-d saliency detection via conditional variational autoencoders,” in *Proceedings of the IEEE/CVF Conference on Computer Vision and Pattern Recognition*, 2020, pp. 8582–8591.
- [32] C. Li, R. Cong, Y. Piao, Q. Xu, and C. C. Loy, “Rgb-d salient object detection with cross-modality modulation and selection,” in *European Conference on Computer Vision*. Springer, 2020, pp. 225–241.
- [33] G. Li, Z. Liu, and H. Ling, “Icnnet: Information conversion network for rgb-d based salient object detection,” *IEEE Transactions on Image Processing*, vol. 29, pp. 4873–4884, 2020.
- [34] H. Chen, Y. Deng, Y. Li, T.-Y. Hung, and G. Lin, “Rgbd salient object detection via disentangled cross-modal fusion,” *IEEE Transactions on Image Processing*, vol. 29, pp. 8407–8416, 2020.
- [35] W. Ji, J. Li, M. Zhang, Y. Piao, and H. Lu, “Accurate rgb-d salient object detection via collaborative learning,” in *ECCV*, 2020.
- [36] Z. Bai, Z. Liu, G. Li, L. Ye, and Y. Wang, “Circular complement network for rgb-d salient object detection,” *Neurocomputing*, vol. 451, pp. 95–106, 2021.
- [37] J.-X. Zhao, Y. Cao, D.-P. Fan, M.-M. Cheng, X.-Y. Li, and L. Zhang, “Contrast prior and fluid pyramid integration for rgbd salient object detection,” in *Proceedings of the IEEE Conference on Computer Vision and Pattern Recognition*, 2019, pp. 3927–3936.
- [38] D.-P. Fan, Y. Zhai, A. Borji, J. Yang, and L. Shao, “Bbs-net: Rgb-d salient object detection with a bifurcated backbone strategy network,” in *European Conference on Computer Vision (ECCV)*, 2020.
- [39] Y. Piao, W. Ji, J. Li, M. Zhang, and H. Lu, “Depth-induced multi-scale recurrent attention network for saliency detection,” in *Proceedings of the IEEE International Conference on Computer Vision*, 2019, pp. 7254–7263.
- [40] Y. Cheng, H. Fu, X. Wei, J. Xiao, and X. Cao, “Depth enhanced saliency detection method,” in *Proceedings of international conference on internet multimedia computing and service*, 2014, pp. 23–27.
- [41] C. Zhu, G. Li, W. Wang, and R. Wang, “An innovative salient object detection using center-dark channel prior,” in *Proceedings of the IEEE International Conference on Computer Vision Workshops*, 2017, pp. 1509–1515.
- [42] L.-C. Chen, Y. Yang, J. Wang, W. Xu, and A. L. Yuille, “Attention to scale: Scale-aware semantic image segmentation,” in *Proceedings of the IEEE conference on computer vision and pattern recognition*, 2016, pp. 3640–3649.
- [43] H. Zhao, J. Shi, X. Qi, X. Wang, and J. Jia, “Pyramid scene parsing network,” in *Proceedings of the IEEE conference on computer vision and pattern recognition*, 2017, pp. 2881–2890.
- [44] K. Desingh, K. M. Krishna, D. Rajan, and C. Jawahar, “Depth really matters: Improving visual salient region detection with depth,” in *Proceedings of the British Machine Vision Conference (BMVC)*, 2013.
- [45] H. Song, Z. Liu, H. Du, G. Sun, O. Le Meur, and T. Ren, “Depth-aware salient object detection and segmentation via multiscale discriminative saliency fusion and bootstrap learning,” *IEEE Transactions on Image Processing*, vol. 26, no. 9, pp. 4204–4216, 2017.
- [46] T. Zhou, D.-P. Fan, M.-M. Cheng, J. Shen, and L. Shao, “Rgb-d salient object detection: A survey,” *arXiv preprint arXiv:2008.00230*, 2020.
- [47] J. Han, H. Chen, N. Liu, C. Yan, and X. Li, “Cnns-based rgb-d saliency detection via cross-view transfer and multiview fusion,” *IEEE transactions on cybernetics*, vol. 48, no. 11, pp. 3171–3183, 2017.
- [48] G. Li, Z. Liu, M. Chen, Z. Bai, W. Lin, and H. Ling, “Hierarchical alternate interaction network for rgb-d salient object detection,” *IEEE Transactions on Image Processing*, vol. 30, pp. 3528–3542, 2021.
- [49] M.-M. Cheng, N. J. Mitra, X. Huang, P. H. Torr, and S.-M. Hu, “Global contrast based salient region detection,” *IEEE Transactions on Pattern Analysis and Machine Intelligence*, vol. 37, no. 3, pp. 569–582, 2014.
- [50] D. A. Klein and S. Frintrop, “Center-surround divergence of feature statistics for salient object detection,” in *2011 International Conference on Computer Vision*. IEEE, 2011, pp. 2214–2219.
- [51] G. Li, Z. Liu, R. Shi, Z. Hu, W. Wei, Y. Wu, M. Huang, and H. Ling, “Personal fixations-based object segmentation with object localization and boundary preservation,” *IEEE Transactions on Image Processing*, vol. 30, pp. 1461–1475, 2020.
- [52] J.-X. Zhao, J.-J. Liu, D.-P. Fan, Y. Cao, J. Yang, and M.-M. Cheng, “Egnet: Edge guidance network for salient object detection,” in *Proceedings of the IEEE International Conference on Computer Vision*, 2019, pp. 8779–8788.
- [53] C. Wang, J. Miguel Buenaposada, R. Zhu, and S. Lucey, “Learning depth from monocular videos using direct methods,” in *Proceedings of the IEEE Conference on Computer Vision and Pattern Recognition*, 2018, pp. 2022–2030.
- [54] R. Garg, V. K. BG, G. Carneiro, and I. Reid, “Unsupervised cnn for single view depth estimation: Geometry to the rescue,” in *European Conference on Computer Vision*. Springer, 2016, pp. 740–756.
- [55] D. Eigen, C. Puhrsch, and R. Fergus, “Depth map prediction from a single image using a multi-scale deep network,” in *Advances in neural information processing systems*, 2014, pp. 2366–2374.
- [56] D. Eigen and R. Fergus, “Predicting depth, surface normals and semantic labels with a common multi-scale convolutional architecture,” in *Proceedings of the IEEE international conference on computer vision*, 2015, pp. 2650–2658.
- [57] I. Laina, C. Rupprecht, V. Belagiannis, F. Tombari, and N. Navab, “Deeper depth prediction with fully convolutional residual networks,” in *2016 Fourth international conference on 3D vision (3DV)*. IEEE, 2016, pp. 239–248.
- [58] H. Fu, M. Gong, C. Wang, K. Batmanghelich, and D. Tao, “Deep ordinal regression network for monocular depth estimation,” in *Proceedings of the IEEE Conference on Computer Vision and Pattern Recognition*, 2018, pp. 2002–2011.
- [59] W. Yin, Y. Liu, C. Shen, and Y. Yan, “Enforcing geometric constraints of virtual normal for depth prediction,” in *Proceedings of the IEEE International Conference on Computer Vision*, 2019, pp. 5684–5693.
- [60] K. Simonyan and A. Zisserman, “Very deep convolutional networks for large-scale image recognition,” in *International Conference on Learning Representations*, May 2015.
- [61] L. He, H. Zhu, F. Li, H. Bai, R. Cong, C. Zhang, C. Lin, M. Liu, and Y. Zhao, “Towards fast and accurate real-world depth super-resolution: Benchmark dataset and baseline,” in *IEEE Conference on Computer Vision and Pattern Recognition (CVPR)*, 2021, pp. 9229–9238.
- [62] A. Mousavian, H. Pirsiavash, and J. Košecká, “Joint semantic segmentation and depth estimation with deep convolutional networks,” in *2016 Fourth International Conference on 3D Vision (3DV)*. IEEE, 2016, pp. 611–619.
- [63] N. Liu, N. Zhang, and J. Han, “Learning selective self-mutual attention for rgb-d saliency detection,” in *Proceedings of the IEEE/CVF Conference on Computer Vision and Pattern Recognition*, 2020, pp. 13756–13765.
- [64] X. Zhang, T. Wang, J. Qi, H. Lu, and G. Wang, “Progressive attention guided recurrent network for salient object detection,” in *Proceedings of the IEEE Conference on Computer Vision and Pattern Recognition*, 2018, pp. 714–722.
- [65] J. Hu, L. Shen, and G. Sun, “Squeeze-and-excitation networks,” in *Proceedings of the IEEE conference on computer vision and pattern recognition*, 2018, pp. 7132–7141.
- [66] L. Chen, H. Zhang, J. Xiao, L. Nie, J. Shao, W. Liu, and T.-S. Chua, “Sca-cnn: Spatial and channel-wise attention in convolutional networks for image captioning,” in *Proceedings of the IEEE conference on computer vision and pattern recognition*, 2017, pp. 5659–5667.
- [67] Z. Chen, Q. Xu, R. Cong, and Q. Huang, “Global context-aware progressive aggregation network for salient object detection,” in *AAAI Conference on Artificial Intelligence (AAAI)*, 2020, pp. 10599–10606.
- [68] C. Zhu and G. Li, “A three-pathway psychobiological framework of salient object detection using stereoscopic technology,” in *Proceedings of the IEEE International Conference on Computer Vision Workshops*, 2017, pp. 3008–3014.
- [69] C. Yang, L. Zhang, H. Lu, X. Ruan, and M.-H. Yang, “Saliency detection via graph-based manifold ranking,” in *Proceedings of the IEEE*

- conference on computer vision and pattern recognition*, 2013, pp. 3166–3173.
- [70] Y. Li, X. Hou, C. Koch, J. M. Rehg, and A. L. Yuille, “The secrets of salient object segmentation,” in *Proceedings of the IEEE Conference on Computer Vision and Pattern Recognition*, 2014, pp. 280–287.
- [71] A. Borji, M.-M. Cheng, H. Jiang, and J. Li, “Salient object detection: A benchmark,” *IEEE transactions on image processing*, vol. 24, no. 12, pp. 5706–5722, 2015.
- [72] J. Deng, W. Dong, R. Socher, L.-J. Li, K. Li, and L. Fei-Fei, “Imagenet: A large-scale hierarchical image database,” in *2009 IEEE conference on computer vision and pattern recognition*. Ieee, 2009, pp. 248–255.
- [73] L.-C. Chen, G. Papandreou, I. Kokkinos, K. Murphy, and A. L. Yuille, “Deeplab: Semantic image segmentation with deep convolutional nets, atrous convolution, and fully connected crfs,” *IEEE transactions on pattern analysis and machine intelligence*, vol. 40, no. 4, pp. 834–848, 2017.
- [74] L. Zhang, J. Dai, H. Lu, Y. He, and G. Wang, “A bi-directional message passing model for salient object detection,” in *Proceedings of the IEEE Conference on Computer Vision and Pattern Recognition*, 2018, pp. 1741–1750.
- [75] Z. Deng, X. Hu, L. Zhu, X. Xu, J. Qin, G. Han, and P.-A. Heng, “R3net: Recurrent residual refinement network for saliency detection,” in *Proceedings of the 27th International Joint Conference on Artificial Intelligence*. AAAI Press, 2018, pp. 684–690.
- [76] J.-J. Liu, Q. Hou, M.-M. Cheng, J. Feng, and J. Jiang, “A simple pooling-based design for real-time salient object detection,” in *Proceedings of the IEEE Conference on Computer Vision and Pattern Recognition*, 2019, pp. 3917–3926.